ACS Photonics

Letter

Cite This: ACS Photonics XXXX, XXX, XXX−XXX

pubs.acs.org/journal/apchd5

Pushing Down the Limit: In Vitro Detection of a Polypeptide Monolayer on a Single Infrared Resonant Nanoantenna

Rostyslav Semenyshyn,[†,§] Florian Mörz,[*,†,§] Tobias Steinle,[†] Monika Ubl,[†] Mario Hentschel,[†] Frank Neubrech,[‡] and Harald Giessen[†]

[†]4th Physics Institute and Research Center SCoPE, University of Stuttgart, Pfaffenwaldring 57, 70569 Stuttgart, Germany

[‡]Kirchhoff Institute for Physics, University of Heidelberg, Im Neuenheimer Feld 227, 69120 Heidelberg, Germany

Supporting Information

ABSTRACT: Infrared vibrational spectroscopy is a powerful tool for the identification of changes of the secondary protein structure, which are associated with many human diseases, such as Alzheimer's or Parkinson's disease. In order to obtain deeper insight into the mechanisms that lead to such changes, it is important to investigate the protein conformation on minimum sample concentrations and volumes, ideally on the single-protein level, and at short measurement times. For this purpose, surface-enhanced infrared absorption in combination with Fourier-transform infrared (FTIR) micro-spectroscopy is a highly suitable technique, but is usually limited to large numbers of proteins and long integration times due to the low brilliance of the standard thermal infrared light sources, such as Globar light sources. Here, we push this inherent limit down by using a highly brilliant, broadband mid-IR laser in combination with a standard FTIR microscope. Thus, detecting the secondary protein structure in a sample volume that is ∼100 times smaller than previously demonstrated becomes feasible with our tabletop FTIR system. We utilize polypeptides as a model system, which we functionalize on a *single* resonant gold nanoantenna, and demonstrate the capabilities of our ultrasensitive system to detect the protein conformation in a living environment within 10 min, without the necessity of frequency tuning the mid-IR laser or any data postprocessing. For comparison, measurements conducted with a synchrotron light source were also performed, which support the results obtained with the laser source. We believe that with further advances it will be possible to scale the process to the ultimate limit of a few or even single proteins and observe the conformational behavior of a few or individual entities in an aqueous environment.

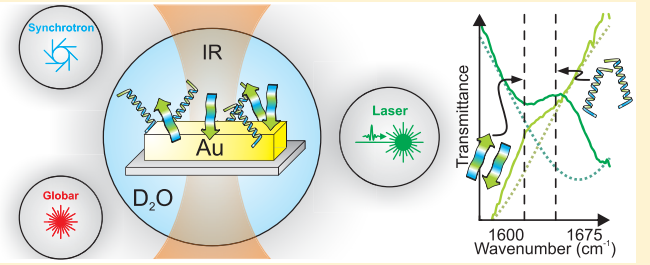

KEYWORDS: *plasmonics, surface-enhanced infrared absorption spectroscopy, proteins, conformational changes, biosensing*

The number of people suffering from type II diabetes, Alzheimer's, or Parkinson's disease is increasing as a consequence of a higher average life expectancy and the lifestyle in today's world.[1] These diseases are just a few examples of diseases that are associated with protein misfolding,[2,3] such as the folding from the α-helix to the β-sheet configuration. However, there is no successful treatment of such diseases, as, among many other things, the folding mechanism is not well understood yet.[1] One reason is the lack of diagnostic tools that allow fundamental research on a daily basis at high speed, with high sensitivity and reliability. A possibility to investigate protein folding is Fourier-transform infrared (FTIR) spectroscopy in the fingerprint spectral region.[4−7] Standard tabletop systems usually require high concentrations, which do not allow the analysis of only a few proteins in order to study the individual reaction on different stimuli, due to a relatively low brilliance of the typically used thermal light sources, such as Globar light sources. Understanding the interactions of individual molecules during physiological processes would provide more insight into the mechanisms that trigger the molecule to undergo certain conformational and thus functional changes. The detection sensitivity has recently been increased significantly by using surface-enhanced infrared absorption (SEIRA) spectroscopy in FTIRs, which takes advantage of strong near-fields of plasmonic nanoantenna arrays that are resonant to the vibration.[8−11] Thus, the protein signal can be enhanced by several orders of magnitude and appears with a Fano-type line shape on top of the antenna profile.[12] Reaching the single-molecule level by exploiting plasmonic enhancement has been demonstrated in Raman spectroscopy,[13] but has not been achieved in FTIR spectroscopy yet. Recent publications demonstrate the high potential of this approach by in vitro monitoring protein folding using antenna fields for signal enhancement.[14−17] Despite a significant increase of measurement sensitivity, the amount of detected proteins on the plasmonic nanoarrays is still on the order of hundreds of thousands of proteins. The sensitivity can be further improved by using synchrotron light sources, which exhibit an orders of

Received: August 6, 2019
Published: October 22, 2019

DOI: 10.1021/acsphotonics.9b01125
ACS Photonics XXXX, XXX, XXX−XXX

magnitude higher brilliance,[18−20] but at the expense of limited availability, accessibility, and high costs.

In contrast to these far-field techniques, one can use atomic force (AFM)[21] or scanning near-field optical (SNOM)[22−26] microscopy to detect vibrations on a few-protein level. However, these approaches impede in vitro measurements, although first results have been obtained due to focused efforts. Currently, one needs to decide between in vitro detection using relatively large concentrations in far-field spectroscopy and investigations on the few-protein level, applying near-field optical microscopes.

The key element to further enhance the measurement sensitivity is the application of a mid-IR light source, which exhibits a brilliance that exceeds that of synchrotrons, which has good beam quality (ideally TEM_{00}) and a high coherence to enable efficient sample illumination. Furthermore, a single source is required, whose bandwidth is sufficiently broad to detect the desired molecular vibrations at once, avoiding the necessity for spectral sweeping. Light sources that can match these requirements are mid-IR lasers with ultrashort and hence broadband pulses.[27−29]

In this work, we demonstrate a combination of a highly brilliant, pulsed laser source and an *individual* plasmonic nanoantenna as an ultrasensitive platform for tabletop protein studies at attomolar concentrations and attoliter volumes.[8,30] Our light source is based on tunable parametric frequency conversion, which covers a broad spectral tuning range from 1.33 to 8 μm (7500−1250 cm^{-1}). The laser pulses exhibit a bandwidth of about 125 cm^{-1} ($1/e^2$-width), which is sufficient to cover molecular amide-I vibrations without frequency tuning. A detailed discussion can be found in refs 31−34. We investigate in vitro the conformation of polypeptide monolayers on single gold nanoantennas, thus exploiting the plasmonic signal enhancement of SEIRA. As control experiments, we additionally apply a synchrotron and a Globar as light source, which commonly are the workhorses in FTIR spectroscopy. Figure 1 depicts the experimental procedure. For in vitro measurements a microfluidic cell is used, allowing transmission measurements and control of the liquid environment.

RESULTS AND DISCUSSION

The measurement setup consists of a Bruker Vertex 80 FTIR spectrometer, which is attached to a Bruker Hyperion 2000 microscope. During all experiments, we use a 36× condenser and objective for illuminating the measured sample area, which is limited to about 10 × 10 μm^2 via the microscope aperture. A liquid nitrogen cooled MCT (MCT D313) detector is employed for detection, and spectra are measured at 4 cm^{-1} resolution. The FTIR includes a Globar and offers an external light source input, which we use for laser incoupling. The setup is flushed with nitrogen to minimize atmospheric absorptions to a negligible extent. The measurements applying a synchrotron light source were conducted at the Swiss Light Source at Paul Scherrer Insitute in Villigen, Switzerland, at a similar Bruker FTIR microscope setup.[35]

A microfluidic cell is constructed for in vitro detection, enabling transmission measurements and control of the liquid environment. During the presented experiments, D_2O-based solutions are used, as H_2O exhibits vibrational features in the same spectral range as the polypeptides.[15]

The utilized gold nanoantennas differ in length to ensure the plasmonic resonance matches the polypeptide resonance for

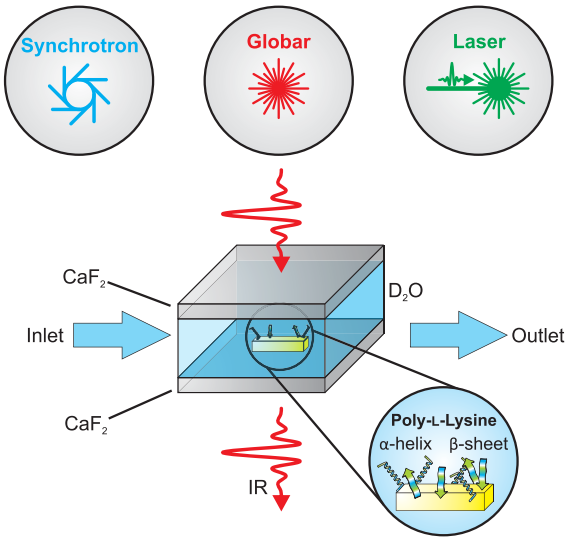

Figure 1. Schematic drawing of the experimental procedure. The conformation of a polypeptide monolayer on a single gold nanoantenna is investigated in vitro, employing SEIRA and FTIR spectroscopy. To reach such a high sensitivity, we utilize a synchrotron light source for reference measurements and a tunable mid-IR laser in a combination with a Globar for tabletop experiments.

efficient near-field enhancement.[36] The resulting antennas are about 100 nm in height and width and between 1.7 and 1.9 μm long and placed on a CaF_2 substrate. Here, we limit the discussion to the antennas exhibiting optimum signal enhancement, whereas further measurements are given in the Supporting Information. The antenna length might vary between the presented measurements, due to the different light sources and samples. In refs 14−16 similar antenna geometries have been used in large antenna arrays, providing a good comparison to our results. Further advances in the antenna design might improve the plasmonic signal enhancement if a laser light source is used, as the overlap with the laser intensity profile could be optimized. However, this is beyond the scope of this work.

A suitable model system for the secondary structure analysis is poly-L-lysine (PLL).[37,38] Similar to many proteins, it exhibits different conformations, and by analyzing the so-called amide-I vibrations, structural changes can be detected. Spectral features shift in frequency and differ in spectral shape as the conformation changes, due to the rearrangement of intramolecular bindings. We particularly focus on the detection of the so-called α-helical and β-sheet PLL conformations, which exhibit resonance peaks at around 1648 and 1618 cm^{-1},[15,39] respectively. The recipe of the functionalization procedure is taken from literature[39] and has been modified to our purposes in previous studies.[15,40] More information can be found in the Supporting Information. The estimated number of molecules contributing to a plasmonically enhanced signal is 1600 for a *single* antenna,[15] assuming that only molecules in the vicinity of the tip ends, where the near-field is highest, contribute to the polypeptide signal.[41]

The adsorption of PLL is conducted in a neutral environment; thus a random distribution of both conformations is expected, which is to be investigated.[15,39] However, if the sample is placed in a D_2O-based sodium dodecyl sulfate (SDS) solution, the polypeptides denaturate and mostly fold

DOI: 10.1021/acsphotonics.9b01125
ACS Photonics XXXX, XXX, XXX−XXX

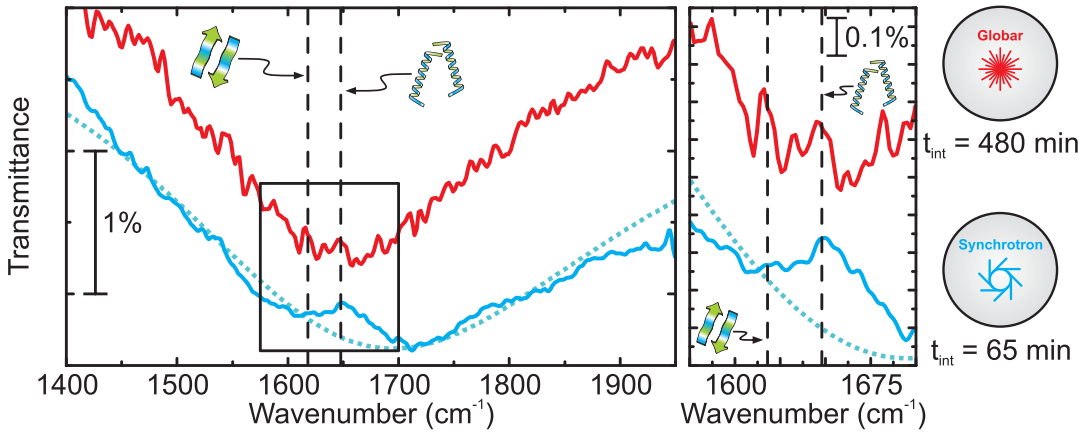

Figure 2. Comparison between synchrotron and Globar spectra of the polypeptide-covered single antenna. A 1.80 μm long antenna is used for the synchrotron measurement, whereas a 1.75 μm long antenna is used for the Globar. The spectra are shifted in transmittance for better comparability, and the bare profile of a 1.80 μm long antenna measured with the synchrotron is indicated in a short-dotted line. The inset (magnified in the right panel) gives a more detailed view on the region of interest. A distinct signal is observed with the synchrotron matching the α-helical resonance peak. The Globar noise is significantly higher due to its lower brilliance and exceeds the expected signal. No β-sheet signal is observed in either case. The α-helical and β-sheet polypeptide resonances are indicated by vertical long-dashed lines at around 1648 and 1618 cm^{-1}.

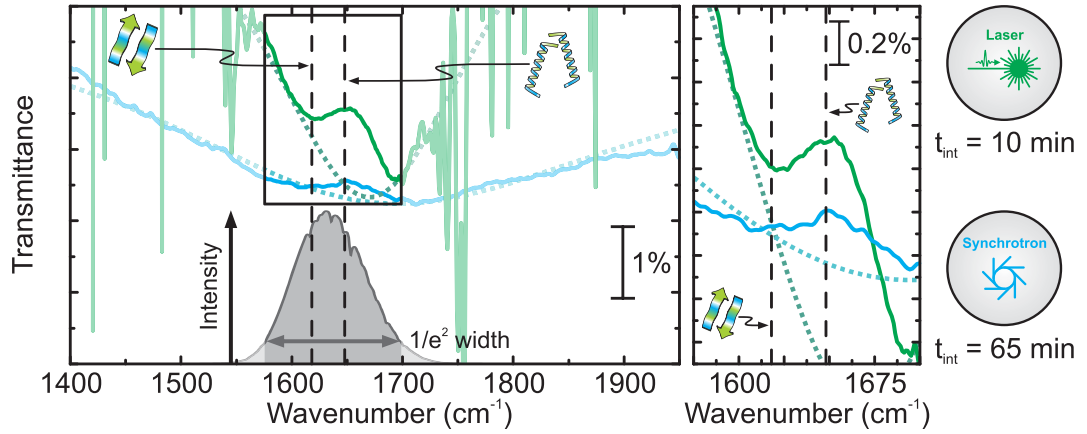

Figure 3. Investigation of the polypeptide sample using the synchrotron and laser. A typical laser intensity distribution is depicted in gray, measured in transmission through the bare CaF_2 substrate (background measurement). The $1/e^2$-bandwidth reaches 125 cm^{-1}, allowing both polypeptide conformations to be detected equally well. Outside that range a too low intensity is available for detection. Note that the spectra are shifted in the y-direction for better comparability. For a better visibility of the polypeptide resonances overlaying the antenna profiles, the bare antenna profiles are indicated as short-dotted lines. The right panel, which is the magnified inset from the left panel, depicts a zoom-in view. Both spectra exhibit a distinct and similar resonance at 1648 cm^{-1} on top of the antenna profile, which matches the α-helical amide-I vibration. The laser exhibits a significantly higher signal strength at a 6 times lower measurement time. The SNR reaches 58, compared to 13 using the synchrotron. The α-helical and β-sheet polypeptide resonances are indicated by vertical long-dashed lines at around 1648 and 1618 cm^{-1}.

into the β-sheet conformation.[42−44] Thus, we want to make sure to detect both α-helical and β-sheet signals.

To validate our sensing concept, we first perform reference measurements using light sources that may fully cover the plasmonic resonance of the functionalized antenna. Therefore, the first measurements are conducted using a Globar and the synchrotron light source. Figure 2 depicts the recorded spectra of a 1.80 μm long antenna, covered with molecules (synchrotron measurement) and a slightly shorter antenna of 1.75 μm length (Globar measurement), exhibiting broad plasmonic resonances with center frequencies of about 1700 and 1650 cm^{-1}, respectively. A detailed view on the spectral region of interest is given next to the full spectra. The spectrum measured with the Globar clearly exhibits high noise, which exceeds any expected PLL signal. In contrast, the signal-to-noise ratio (SNR) of the synchrotron spectrum is significantly higher, and a distinct resonance stands out from the spectrum, despite a significantly shorter measurement time compared to the Globar. For a better visibility of this feature, we indicate the bare antenna resonance in a short-dotted line. This bare antenna profile is obtained by a Lorentzian fitting method (see Supporting Information). The signal exactly matches the spectral position of the amide-I vibration at around 1648 cm^{-1}, which is characteristic for an α-helical polypeptide conformation and reaches an SNR of approximately 13. Further information regarding the calculation of the SNR is given in the Supporting Information. Figure 2 also marks the position of the β-sheet resonance at 1618 cm^{-1}. Here, no signal is detected, and we conclude the PLL monolayer to be predominantly in the α-helical conformation. Our measurement matches the expected polypeptide responses given in refs 15 and 16, where similar studies have been conducted on large antenna fields. To determine the sensitivity of the synchrotron light source, we calculated the RMS noise in the given spectral

DOI: 10.1021/acsphotonics.9b01125
ACS Photonics XXXX, XXX, XXX−XXX

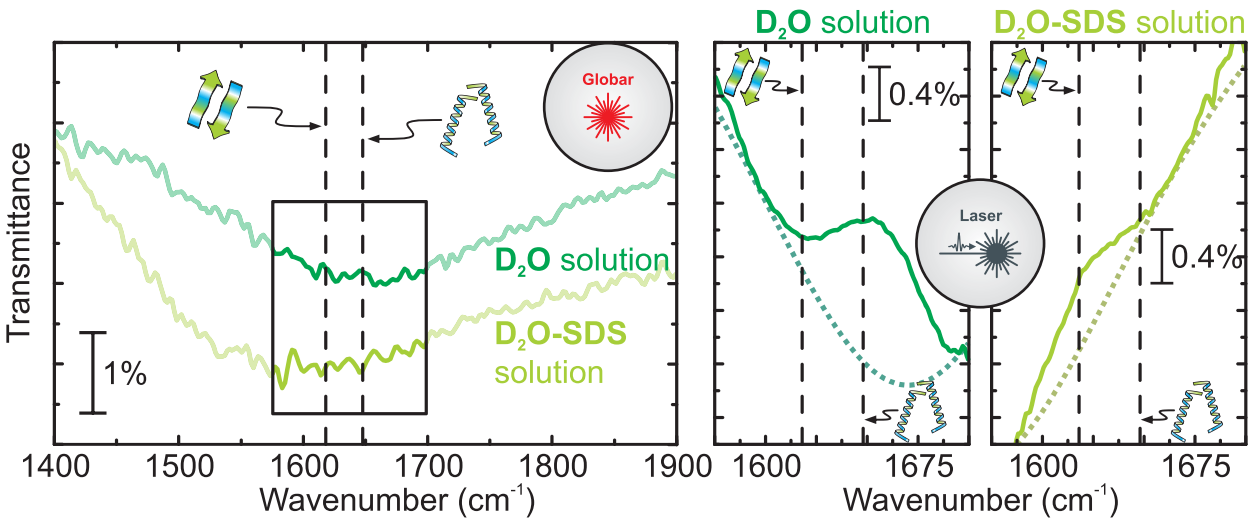

Figure 4. Comparison of measurements conducted in D_2O (dark green) and D_2O−SDS (light green) solutions. Whereas both PLL conformations can be present in the first case, the polypeptides are expected to be mainly in the β-sheet state in the latter case. Antenna spectra that are recorded with the Globar in order to characterize the antenna resonances in the different liquid environments are depicted in the left panel. The antenna resonance of the 1.80 μm long antenna, measured in D_2O−SDS, is found at ∼1600 cm^{-1}. The right two panels of the figure depict the inset region of the left panel, when investigated with the laser source, including Lorentzian fits (see Supporting Information) of the bare antenna background as short-dotted lines. In contrast to the measurement in D_2O solution (dark green), which only exhibits a strong α-helical signal, a broad peak in the vicinity of the β-sheet resonance is visible in D_2O−SDS solution (light green). Furthermore, no α-helical signal is detected in D_2O−SDS, as expected as a consequence of the denaturation of the polypeptides. This indicates that the polypeptide monolayer is predominantly in the β-sheet conformation. From these observations, we conclude that both conformations can be distinguished well with the laser source. All spectra are shifted in the y-direction for a better comparability. The α-helical and β-sheet polypeptide resonances are indicated by vertical long-dashed lines at around 1648 and 1618 cm^{-1}.

region for single spectra. Assuming the single shot detection limit, i.e., the sensitivity, is reached at an SNR of 1, a signal amplitude of 0.23% is required to be detected. In contrast to the sensitivity, we define the detection limit to be dependent on the integration time. Further information is given in the Supporting Information. We would like to point out that our definition might not be valid in general, but it is a comprehensible measure for the presented data.

To make this concept feasible for tabletop applications, we continue our studies utilizing the laser light source. For the further experiments, the laser is tuned to a center frequency of 1634 cm^{-1}, which is in between the α-helical and β-sheet resonances. Figure 3 depicts a typical spectral intensity distribution, shown in gray, as an inset in the main figure. The semitransparent areas mark the spectral range that is not covered by the laser light. In this range the remaining laser intensity is too low to be detected and the FTIR spectra are dominated by noise. Only minor atmospheric absorptions are visible as a consequence of the nitrogen purge. Following Figure 2, we compare the measurement obtained with the laser to the synchrotron spectrum. We employ a 1.75 μm long antenna for the laser measurement, as we did using the Globar. The antenna profiles are fitted using a Lorentzian fit (see Supporting Information) and are indicated as short-dotted lines.

Comparing the slopes of the synchrotron and laser spectra, the latter appears steeper, as well as blue-shifted. This is related to the slightly shorter antenna length and the different illumination geometries. Considering the different beam shapes and qualities of the light sources, a higher light intensity at the sample position, as well as a higher optical throughput, is achieved with the laser, compared to the synchrotron and Globar. This results in a significantly higher intensity reaching the detector, leading to a better SNR. It needs to be considered that the plasmonic resonance can slightly shift, depending on the illumination of the antenna, i.e., plane wave or angled illumination.[45]

On the right-hand side of Figure 3, a detailed view on the region of interest ($1/e^2$ laser bandwidth) is given. Here, the laser spectrum exhibits a distinct vibrational signal on top of the antenna profile, which agrees well with the synchrotron measurement, however, with a much better SNR of 58. The signal also agrees well with literature data.[15,16] The signal fits the resonance of the α-helical amide-I vibration well, whereas no signal at the expected β-sheet signal is observed. This indicates an α-helical conformation of the PLL monolayer.

Besides the better SNR compared to the synchrotron, the laser allows measurements within less than 6 times the measurement time. Here, spectra are accumulated for 10 min, although 2.5 min is sufficient to achieve an SNR comparable to the synchrotron spectrum, as shown in the Supporting Information. The single-shot sensitivity is reached at 0.23% absorption, which is similar to the synchrotron single-shot sensitivity. After 10 min integration time the detection limit reaches 0.02%, and after 25 min it is at 0.015% absorption. In comparison, the synchrotron detection limit is at 0.03% using a 10 min integration time and saturates at 0.019% after approximately 30 min. The excellent detection limits and sensitivities for both synchrotron and laser highlight the potential of these light sources. The dominant noise sources of the laser in long-term measurements are minimum wavelength and power fluctuations, despite the very good long-term stability of the laser as measured in ref 33 and mechanical fluctuations of the microscope. The significant difference in SNR between laser and synchrotron is mainly due to the high signal amplitude, which we attribute to the higher brilliance of the laser. We believe that fast measurements with excellent SNR are of high importance, and a tabletop setup is required

DOI: 10.1021/acsphotonics.9b01125
ACS Photonics XXXX, XXX, XXX−XXX

to conduct research on a daily basis at moderate cost and effort, which is enabled with the presented approach.

So far, we conclude that the PLL monolayer on the investigated antennas is predominantly in the α-helical conformation. In a next step, we prepare a sample in the β-sheet state by adding SDS to the D_2O solution in order to examine the distinguishability of the individual conformations. Initially, the sample is investigated employing the Globar and spectra are accumulated for about 8 h. Figure 4 depicts the measured spectrum (light green) in the left panel. In the D_2O−SDS environment, we utilized a 1.80 μm long antenna. For a better comparison to the previous measurements, the Globar spectrum (dark green) of the 1.75 μm long antenna measured in D_2O is also plotted (dark green). The 1.80 μm long antenna spectrum exhibits a higher noise level, as a consequence of the added SDS to the D_2O environment, which exhibits OH vibrations in the considered frequency range, adding noise to the spectrum. Please note that no vibrational modes can be identified in the spectra taken with the Globar, as expected.

Next, the sample is investigated employing the laser light source, and the spectra are depicted in the right two panels of Figure 4, including Lorentzian fits of the bare antenna resonances (see Supporting Information) to visualize the polypeptide signals. The measurement in D_2O solution is plotted in dark green. This is the same measurement as previously shown in Figure 3. The measurement conducted in D_2O−SDS is depicted in light green line color. Here, a broad feature close to the expected β-sheet vibration is visible on top of the antenna resonance, whereas the previously observed strong α-helical signal vanished. This indicates that the polypeptide monolayer mostly folded from the α-helical into the β-sheet conformation. We calculated an SNR of 8, and the single-shot sensitivity is measured to be 0.58%. Compared to the measurements in D_2O, the sensitivity is more than a factor 2 weaker as a consequence of the OH vibrations in the D_2O−SDS environment. After 45 min integration time a detection limit of 0.068% is reached. The lower SNR is due to the weak signal amplitude as a consequence of the denaturated polypeptides. Nevertheless, both conformational vibrations can be detected and distinguished with the laser source, without applying any changes. Several antennas have been investigated in D_2O−SDS solution, but no strong α-helical signal is observed any more, whereas features at the β-sheet resonance became more prominent. An additional antenna measurement is given in the Supporting Information, with evidence for both features. The measured polypeptide signals match the literature data well.[15,16]

In general, several antennas have been investigated, leading to similar results as presented. In the Supporting Information we present measurements performed on antennas of different length, which affects the plasmonic signal enhancement due to a resonance detuning. Due to the sensitive functionalization procedure, the detected protein conformation and signal strength vary between the different samples, but are comparable overall.

CONCLUSION

To conclude, we investigated in vitro polypeptide monolayers on *single* gold nanoantennas exploiting resonant vibrational surface-enhanced infrared absorption spectroscopy. We employed a tunable parametric light source based on a solid-state laser, which additionally brought significant improvements in terms of an increased signal-to-noise ratio and decreased measurement times compared to Globar or synchrotron light sources. We successfully detected resonances attributed to both the α-helical and β-sheet conformation within minutes, without frequency tuning of the light source. Monitoring folding mechanisms is feasible with this laser source, due to the broadband intensity profile compared to other laser sources in the mid-IR range. These results enable studies of species at attomolar[8] concentrations in attoliter volumes on a daily basis with this novel tabletop system. In combination with further advances of nanoantenna designs[46−52] this might enable the detection of even fewer molecules in the future. We believe that our concept opens up opportunities for in vitro investigation of the protein folding mechanism at a few or even single-molecule level in the near future.

ASSOCIATED CONTENT

Supporting Information

The Supporting Information is available free of charge on the ACS Publications website at DOI: 10.1021/acsphotonics.9b01125.

Sample preparation and measurement routine, signal-to-noise and sensitivity determination, additional antenna measurements using Globar and laser light sources in both D_2O and D_2O−SDS environments, temporal evolution of spectra conducted with the laser light source in D_2O, and Lorentzian fitting (PDF)

AUTHOR INFORMATION

Corresponding Author

*E-mail: f.moerz@pi4.uni-stuttgart.de.

ORCID

Rostyslav Semenyshyn: 0000-0001-6818-7500
Florian Mörz: 0000-0002-8198-0236
Mario Hentschel: 0000-0002-6882-4183
Frank Neubrech: 0000-0002-5437-4118

Author Contributions

§R. Semenyshyn and F. Mörz contributed equally.

Notes

The authors declare no competing financial interest.

ACKNOWLEDGMENTS

We thank the Paul Scherrer Institute for the opportunity to perform the measurements at the Swiss Light Source and are thankful to Dr. Hans-Christian Sigg for his assistance and help with measurements. The authors gratefully acknowledge financial support by the ERC Advanced Grant COMPLEXPLAS, ERC PoC 3D Printedoptics, DFG, Baden-Württemberg Stiftung (PROTEINSENS), Carl-Zeiss-Stiftung, MWK BW (ZAQuant, IQST), and BMBF.

REFERENCES

(1) Knowles, T. P. J.; Vendruscolo, M.; Dobson, C. M. The Amyloid State and Its Association with Protein Misfolding Diseases. *Nat. Rev. Mol. Cell Biol.* **2014**, *15* (6), 384−396.

(2) Irwin, D. J.; Lee, V. M. Y.; Trojanowski, J. Q. Parkinson's Disease Dementia: Convergence of α-Synuclein, Tau and Amyloid-β Pathologies. *Nat. Rev. Neurosci.* **2013**, *14* (9), 626−636.

(3) Hieronymus, L.; Griffin, S. Role of Amylin in Type 1 and Type 2 Diabetes. *Diabetes Educ* **2015**, *41*, 47S−56S.

DOI: 10.1021/acsphotonics.9b01125
ACS Photonics XXXX, XXX, XXX−XXX

(4) Barth, A. Infrared Spectroscopy of Proteins. *Biochim. Biophys. Acta, Bioenerg.* **2007**, *1767* (9), 1073−1101.
(5) Jackson, M.; Mantsch, H. H. The Use and Misuse of FTIR Spectroscopy in the Determination of Protein Structure. *Crit. Rev. Biochem. Mol. Biol.* **1995**, *30* (2), 95−120.
(6) Baker, M. J.; Trevisan, J.; Bassan, P.; Bhargava, R.; Butler, H. J.; Dorling, K. M.; Fielden, P. R.; Fogarty, S. W.; Fullwood, N. J.; Heys, K. A.; et al. Using Fourier Transform IR Spectroscopy to Analyze Biological Materials. *Nat. Protoc.* **2014**, *9* (8), 1771−1791.
(7) Levin, I. W.; Bhargava, R. FOURIER TRANSFORM INFRARED VIBRATIONAL SPECTROSCOPIC IMAGING: Integrating Microscopy and Molecular Recognition. *Annu. Rev. Phys. Chem.* **2005**, *56* (1), 429−474.
(8) Neubrech, F.; Pucci, A.; Cornelius, T. W.; Karim, S.; García-Etxarri, A.; Aizpurua, J. Resonant Plasmonic and Vibrational Coupling in a Tailored Nanoantenna for Infrared Detection. *Phys. Rev. Lett.* **2008**, *101* (15), 157403.
(9) Neubrech, F.; Huck, C.; Weber, K.; Pucci, A.; Giessen, H. Surface-Enhanced Infrared Spectroscopy Using Resonant Nanoantennas. *Chem. Rev.* **2017**, *117* (7), 5110−5145.
(10) Vogt, J.; Huck, C.; Neubrech, F.; Toma, A.; Gerbert, D.; Pucci, A. Impact of the Plasmonic Near- and Far-Field Resonance-Energy Shift on the Enhancement of Infrared Vibrational Signals. *Phys. Chem. Chem. Phys.* **2015**, *17* (33), 21169−21175.
(11) Oh, S. H.; Altug, H. Performance Metrics and Enabling Technologies for Nanoplasmonic Biosensors. *Nat. Commun.* **2018**, *9* (1), 5263.
(12) Giannini, V.; Francescato, Y.; Amrania, H.; Phillips, C. C.; Maier, S. A. Fano Resonances in Nanoscale Plasmonic Systems: A Parameter-Free Modeling Approach. *Nano Lett.* **2011**, *11* (7), 2835−2840.
(13) Zhang, Y.; Zhen, Y. R.; Neumann, O.; Day, J. K.; Nordlander, P.; Halas, N. J. Coherent Anti-Stokes Raman Scattering with Single-Molecule Sensitivity Using a Plasmonic Fano Resonance. *Nat. Commun.* **2014**, *5*, 4424.
(14) Etezadi, D.; Warner, J. B.; Ruggeri, F. S.; Dietler, G.; Lashuel, H. A.; Altug, H. Nanoplasmonic Mid-Infrared Biosensor for in Vitro Protein Secondary Structure Detection. *Light: Sci. Appl.* **2017**, *6* (8), e17029−10.
(15) Semenyshyn, R.; Hentschel, M.; Stanglmair, C.; Teutsch, T.; Tarin, C.; Pacholski, C.; Giessen, H.; Neubrech, F. In Vitro Monitoring Conformational Changes of Polypeptide Monolayers Using Infrared Plasmonic Nanoantennas. *Nano Lett.* **2019**, *19* (1), 1−7.
(16) Etezadi, D.; Warner, J. B.; Lashuel, H. A.; Altug, H. Real-Time in Situ Secondary Structure Analysis of Protein Monolayer with Mid-Infrared Plasmonic Nanoantennas. *ACS Sensors* **2018**, *3* (6), 1109−1117.
(17) Adato, R.; Altug, H. In-Situ Ultra-Sensitive Infrared Absorption Spectroscopy of Biomolecule Interactions in Real Time with Plasmonic Nanoantennas. *Nat. Commun.* **2013**, *4*, 2154.
(18) Miller, L. M.; Smith, R. J. Synchrotrons versus Globars, Point-Detectors versus Focal Plane Arrays: Selecting the Best Source and Detector for Specific Infrared Microspectroscopy and Imaging Applications. *Vib. Spectrosc.* **2005**, *38* (1−2), 237−240.
(19) Dumas, P.; Polack, F.; Lagarde, B.; Chubar, O.; Giorgetta, J. L.; Lefrançois, S. Synchrotron Infrared Microscopy at the French Synchrotron Facility SOLEIL. *Infrared Phys. Technol.* **2006**, *49* (1−2), 152−160.
(20) Bosch, R. A. Computed Flux and Brightness of Infrared Edge and Synchrotron Radiation. *Nucl. Instrum. Methods Phys. Res., Sect. A* **2000**, *454* (2−3), 497−505.
(21) Ruggeri, F. S.; Adamcik, J.; Jeong, J. S.; Lashuel, H. A.; Mezzenga, R.; Dietler, G. Influence of the β-Sheet Content on the Mechanical Properties of Aggregates during Amyloid Fibrillization. *Angew. Chem., Int. Ed.* **2015**, *54* (8), 2462−2466.
(22) Amenabar, I.; Poly, S.; Nuansing, W.; Hubrich, E. H.; Govyadinov, A. A.; Huth, F.; Krutokhvostov, R.; Zhang, L.; Knez, M.; Heberle, J.; et al. Structural Analysis and Mapping of Individual Protein Complexes by Infrared Nanospectroscopy. *Nat. Commun.* **2013**, *4*, 2890.
(23) Brehm, M.; Taubner, T.; Hillenbrand, R.; Keilmann, F. Infrared Spectroscopic Mapping of Single Nanoparticles and Viruses at Nanoscale Resolution. *Nano Lett.* **2006**, *6* (7), 1307−1310.
(24) Xu, X. G.; Rang, M.; Craig, I. M.; Raschke, M. B. Pushing the Sample-Size Limit of Infrared Vibrational Nanospectroscopy: From Monolayer toward Single Molecule Sensitivity. *J. Phys. Chem. Lett.* **2012**, *3* (13), 1836−1841.
(25) Huth, F.; Schnell, M.; Wittborn, J.; Ocelic, N.; Hillenbrand, R. Infrared-Spectroscopic Nanoimaging with a Thermal Source. *Nat. Mater.* **2011**, *10* (5), 352−356.
(26) Amarie, S.; Ganz, T.; Keilmann, F. Mid-Infrared Near-Field Spectroscopy *Opt. Express* **2009**, *17* (24), 153−157.
(27) Bensmann, S.; Gaußmann, F.; Lewin, M.; Wüppen, J.; Nyga, S.; Janzen, C.; Jungbluth, B.; Taubner, T. Near-Field Imaging and Spectroscopy of Locally Strained GaN Using an IR Broadband Laser. *Opt. Express* **2014**, *22* (19), 22369.
(28) Maidment, L.; Schunemann, P. G.; Reid, D. T. Molecular Fingerprint-Region Spectroscopy from 5 to 12 μm Using an Orientation-Patterned Gallium Phosphide Optical Parametric Oscillator. *Opt. Lett.* **2016**, *41* (18), 4261.
(29) Mandon, J.; Guelachvili, G.; Picqué, N. Fourier Transform Spectroscopy with a Laser Frequency Comb. *Nat. Photonics* **2009**, *3* (2), 99−102.
(30) Muskens, O.; Christofilos, D.; Del Fatti, N.; Vallée, F. Optical Response of a Single Noble Metal Nanoparticle. *J. Opt. A: Pure Appl. Opt.* **2006**, *8* (4), S264.
(31) Mörz, F.; Steinle, T.; Steinmann, A.; Giessen, H. Multi-Watt Femtosecond Optical Parametric Master Oscillator Power Amplifier at 43 MHz. *Opt. Express* **2015**, *23* (18), 23960.
(32) Mörz, F.; Semenyshyn, R.; Steinle, T.; Neubrech, F.; Zschieschang, U.; Klauk, H.; Steinmann, A.; Giessen, H. Nearly Diffraction Limited FTIR Mapping Using an Ultrastable Broadband Femtosecond Laser Tunable from 1.33 to 8 μm. *Opt. Express* **2017**, *25* (26), 32355.
(33) Steinle, T.; Mörz, F.; Steinmann, A.; Giessen, H. Ultra-Stable High Average Power Femtosecond Laser System Tunable from 1.33 to 20 μm. *Opt. Lett.* **2016**, *41* (21), 4863.
(34) Steinle, T.; Neubrech, F.; Steinmann, A.; Yin, X.; Giessen, H. Mid-Infrared Fourier-Transform Spectroscopy with a High-Brilliance Tunable Laser Source: Investigating Sample Areas down to 5 μm Diameter. *Opt. Express* **2015**, *23* (9), 11105.
(35) Lerch, P.; Quaroni, L.; Wambach, J.; Schneider, J.; Armstrong, D. B.; Rossetti, D.; Mueller, F. L.; Peier, P.; Schlott, V.; Carroll, L.; et al. IR Beamline at the Swiss Light Source. *J. Phys. Conf. Ser.* **2012**, *359* (1), 012003.
(36) Vogt, J.; Huck, C.; Neubrech, F.; Toma, A.; Gerbert, D.; Pucci, A. Impact of the Plasmonic Near- and Far-Field Resonance-Energy Shift on the Enhancement of Infrared Vibrational Signals. *Phys. Chem. Chem. Phys.* **2015**, *17* (33), 21169−21175.
(37) Chittchang, M.; Salamat-Miller, N.; Alur, H. H.; Velde, D. G. V.; Mitra, A. K.; Johnston, T. P. Poly(L-Lysine) as a Model Drug Macromolecule with Which to Investigate Secondary Structure and Microporous Membrane Transport, Part 2: Diffusion Studies. *J. Pharm. Pharmacol.* **2002**, *54* (11), 1497−1505.
(38) Hartman, R.; Schwaner, R. C.; Hermans, J. Beta Poly(l-Lysine): A Model System for Biological Self-Assembly. *J. Mol. Biol.* **1974**, *90* (3), 415−429.
(39) Fallah, M. A.; Stanglmair, C.; Pacholski, C.; Hauser, K. Devising Self-Assembled-Monolayers for Surface-Enhanced Infrared Spectroscopy of PH-Driven Poly- l -Lysine Conformational Changes. *Langmuir* **2016**, *32* (29), 7356−7364.
(40) Semenyshyn, R.; Hentschel, M.; Huck, C.; Vogt, J.; Weiher, F.; Giessen, H.; Neubrech, F. Resonant Plasmonic Nanoslits Enable in Vitro Observation of Single-Monolayer Collagen-Peptide Dynamics. *ACS Sensors* **2019**, *4*, 1966−1972.
(41) D'Andrea, C.; Bochterle, J. J.; Toma, A.; Huck, C.; Neubrech, F.; Messina, E.; Fazio, B.; Maragò, O. M.; Di Fabrizio, E.; Lamy De La

DOI: 10.1021/acsphotonics.9b01125
ACS Photonics XXXX, XXX, XXX−XXX

Chapelle, M.; et al. Optical Nanoantennas for Multiband Spectroscopy. *ACS Nano* **2013**, *7* (4), 3522−3531.
(42) Wang, Y.; Chang, Y. C. Synthesis and Conformational Transition of Surface-Tethered Polypeptide: Poly(L-Lysine). *Macromolecules* **2003**, *36* (17), 6511−6518.
(43) Xu, Q.; Keiderling, T. A. Effect of Sodium Dodecyl Sulfate on Folding and Thermal Stability of Acid-Denatured Cytochrome c: A Spectroscopic Approach. *Protein Sci.* **2004**, *13* (11), 2949−2959.
(44) Gopal, R.; Park, J. S.; Seo, C. H.; Park, Y. Applications of Circular Dichroism for Structural Analysis of Gelatin and Antimicrobial Peptides. *Int. J. Mol. Sci.* **2012**, *13* (3), 3229−3244.
(45) Krauth, J.; Giessen, H.; Hentschel, M. Wavelength-Dependent Third-Harmonic Generation in Plasmonic Gold Nanoantennas: Quantitative Determination of the d-Band Influence. *ACS Photonics* **2018**, *5* (5), 1863−1870.
(46) Sumikura, H.; Wang, T.; Li, P.; Michel, A. K. U.; Heßler, A.; Jung, L.; Lewin, M.; Wuttig, M.; Chigrin, D. N.; Taubner, T. Highly Confined and Switchable Mid-Infrared Surface Phonon Polariton Resonances of Planar Circular Cavities with a Phase Change Material. *Nano Lett.* **2019**, *19* (4), 2549−2554.
(47) Dong, L.; Yang, X.; Zhang, C.; Cerjan, B.; Zhou, L.; Tseng, M. L.; Zhang, Y.; Alabastri, A.; Nordlander, P.; Halas, N. J. Nanogapped Au Antennas for Ultrasensitive Surface-Enhanced Infrared Absorption Spectroscopy. *Nano Lett.* **2017**, *17* (9), 5768−5774.
(48) Brown, L. V.; Yang, X.; Zhao, K.; Zheng, B. Y.; Nordlander, P.; Halas, N. J. Fan-Shaped Gold Nanoantennas above Reflective Substrates for Surface-Enhanced Infrared Absorption (SEIRA). *Nano Lett.* **2015**, *15* (2), 1272−1280.
(49) Tittl, A.; Leitis, A.; Liu, M.; Yesilkoy, F.; Choi, D. Y.; Neshev, D. N.; Kivshar, Y. S.; Altug, H. Imaging-Based Molecular Barcoding with Pixelated Dielectric Metasurfaces. *Science* **2018**, *360* (6393), 1105−1109.
(50) Tittl, A.; John-Herpin, A.; Leitis, A.; Arvelo, E. R.; Altug, H. Metasurface-Based Molecular Biosensing Aided by Artificial Intelligence. *Angew. Chem., Int. Ed.* **2019**, *58*, 2−15.
(51) Gallinet, B.; Martin, O. J. F. Ab Initio Theory of Fano Resonances in Plasmonic Nanostructures and Metamaterials. *Phys. Rev. B: Condens. Matter Mater. Phys.* **2011**, *83* (23), 1−6.
(52) Yang, Y.; Wang, W.; Boulesbaa, A.; Kravchenko, I. I.; Briggs, D. P.; Puretzky, A.; Geohegan, D.; Valentine, J. Nonlinear Fano-Resonant Dielectric Metasurfaces. *Nano Lett.* **2015**, *15* (11), 7388−7393.

DOI: 10.1021/acsphotonics.9b01125
ACS Photonics XXXX, XXX, XXX−XXX